SULFUR HAZES IN GIANT EXOPLANET ATMOSPHERES: IMPACTS ON REFLECTED LIGHT SPECTRA

Peter Gao[1,2,3], Mark S. Marley, and Kevin Zahnle

NASA Ames Research Center
Moffett Field, CA 94035, USA

Tyler D. Robinson[4,5]

Department of Astronomy and Astrophysics
University of California Santa Cruz
Santa Cruz, CA 95064, USA

Nikole K. Lewis

Space Telescope Science Institute
Baltimore, MD 21218, USA

[1]Division of Geological and Planetary Sciences, California Institute of Technology, Pasadena, CA 91125, USA

[2]NASA Postdoctoral Program Fellow

[3]pgao@caltech.edu

[4]Sagan Fellow

[5]NASA Astrobiology Institute's Virtual Planetary Laboratory

ABSTRACT

Recent work has shown that photochemical hazes composed of elemental sulfur and its allotropes may arise in the atmospheres of warm and temperate giant exoplanets due to the photolysis of H_2S. We investigate the impact such a haze would have on an exoplanet's geometric albedo spectrum using a suite of established radiative–convective, cloud, and albedo models, and how this may impact future direct imaging missions. For Jupiter–massed planets, photochemical destruction of H_2S results in the production of ~1 ppmv of S_8 between 100 and 0.1 mbar. The S_8 mixing ratio is largely independent of the stellar UV flux, vertical mixing rates, and atmospheric temperature for expected ranges of those values, such that the S_8 haze mass is dependent only on the S_8 supersaturation, controlled by the local temperature. Nominal haze masses are found to drastically alter a planet's geometric albedo spectrum: whereas a clear atmosphere is dark at wavelengths between 0.5 and 1 μm due to molecular absorption, the addition of a sulfur haze boosts the albedo there to ~0.7 due to its purely scattering nature. Strong absorption by the haze shortward of 0.4 μm results in albedos <0.1, contrasting the high albedos produced by Rayleigh scattering in a clear atmosphere. The albedo change due to a sulfur haze is largely independent of the location of the haze in the atmosphere, but is a strong function of the haze optical depth as controlled by its column number density and mean particle size, though the absorption feature at short wavelengths remains robust. Detection of such a haze by future direct imaging missions like WFIRST is possible, though discriminating between a sulfur haze and any other reflective material, such as water ice, will require observations shortward of 0.4 μm, which is currently beyond WFIRST's grasp.

Keywords: planets and satellites: atmospheres

1. INTRODUCTION

Observations of exoplanet atmospheres have revealed a ubiquity of clouds and hazes that impede understanding of atmospheric composition (Gibson et al. 2012, 2013; Deming et al. 2013; Jordán et al. 2013; Mandell et al. 2013; Sing et al. 2013; Chen et al. 2014; Schlawin et al. 2014; Wilkins et al. 2014; Fukui et al. 2014; Mallonn & Strassmeier 2016).

Their presence is typically shown by a flattening of spectral features in the transmission spectrum, resulting from the inability of stellar photons to reach depths in the atmosphere below the cloud and haze layers. Such flat transmission spectra have been seen across many exoplanets of different sizes, effective temperatures, and stellar irradiation levels (e.g. Crossfield et al. 2013; Kreidberg et al. 2014; Knutson et al. 2014a,b; Sing et al. 2016), suggesting that the processes governing cloud and haze formation in exoplanet atmospheres are complex.

One key unknown is whether the particulates blocking the stellar photons are part of a cloud, which condensed from atmospheric gases and are typically supported in an atmosphere by turbulent mixing, or part of a haze, which are produced high in the atmosphere, usually via photochemistry. Morley et al. (2013) showed that, for the super Earth GJ 1214 b, photochemical hazes may be preferred as a solution to its flat transmission spectra, as it is formed high up in the atmosphere. By contrast, cloud particles must be lofted by turbulent mixing, and a high metallicity may be required to ensure enough material gets to the pressure levels probed by transmission spectroscopy to make a difference.

Knowing whether a planet is shrouded by clouds or hazes (or both) is important despite the flat transmission spectra that both types of aerosols generate, as more discriminating features may appear in direct imaging, which is receiving more priority in upcoming missions such as JWST and WFIRST (Beichman et al. 2014; Robinson et al. 2016). Morley et al. (2015) showed, for example, that there are large differences in the reflected light spectra of super Earths depending on whether the planet is cloudy or hazy, and what kind of clouds/hazes are present. Specifically, they showed that cooler planets may be more reflective due to KCl, ZnS, and water clouds, while planets with complex hydrocarbon, "soot" hazes resulting from methane photolysis and polymerization tend to be very dark. Additionally, hazes composed of tholins–thought to be the composition of Titan's hazes (Khare et al. 1984)–are dark at the blue end of the visible range and more reflective at the red end. The reflectivity of clouds and hazes impact the amount of compositional information that can be retrieved from direct imaging, as reflected light is only able to sample the atmosphere above the cloud/haze deck. If the cloud/haze deck is at high altitudes, then the column optical depth of absorbing gases that direct imaging can sample is small, thereby reducing the magnitude of their spectral features in these planets' reflected light spectra (Marley et al. 1999). Likewise, if the cloud/haze is absorbing, then very few photons can sample the chemical composition of the atmosphere and escape.

An alternative set of compounds that are known to form hazes in planetary atmospheres are those derived from sulfur chemistry. In oxidizing atmospheres, SO_2, OCS, and H_2S from volcanic outgassing is transformed into sulfuric acid through photolysis and reactions with water. Condensation of sulfuric acid can then form clouds and hazes, such as the global cloud deck of Venus (Hansen & Hovenier 1974) and the Junge layer in the upper stratosphere of Earth (Junge 1963). In reducing atmospheres, photolysis of H_2S can lead to the formation of elemental sulfur. Hu et al. (2013), for example, showed that terrestrial worlds with H_2–dominated atmospheres can be enveloped in optically thick sulfur hazes resulting from volcanic outgassing of H_2S.

More recent work by Zahnle et al. (2016) showed that rich sulfur photochemistry could potentially take place in the atmospheres of temperate giant exoplanets (250 K $< T <$ 700 K), generating sulfur allotropes that may form hazes at lower temperatures. As these planets are the targets of current and planned direct imaging campaigns, it is essential that the optical characteristics of elemental sulfur hazes be known in order to inform these future observations. In this paper we investigate the geometric albedo spectra of elemental sulfur hazes and their variations with haze properties, such as the location of the haze in the atmosphere and the haze optical depth. We also address the observability of a sulfur haze for the upcoming space–based direct imaging campaigns of WFIRST (Spergel et al. 2013).

In §2, we give an overview of the sulfur chemistry elaborated upon in Zahnle et al. (2016), with a focus towards the formation of sulfur hazes, as well as sulfur's optical properties. In §3 we describe in brief the suite of models used in this study. In §4 we present our results showing how the geometric albedo varies with different haze properties and whether a clear planet can be distinguished from a hazy planet using proposed instruments onboard WFIRST. Finally, in §5 we discuss the impact of our assumptions, the implications of our results, and potential avenues of investigation for future missions and observation campaigns.

2. SULFUR IN GIANT EXOPLANETS

In temperate and warm giant exoplanet atmospheres (T $\sim$ 250–700 K), sulfur is found mostly in the form of H_2S. Transport of H_2S to the tropopause by turbulent mixing and advection then allows for its destruction by photolysis and reactions with atomic H resulting from photolysis of CH_4, NH_3, and H_2O (Zahnle et al. 2016)

$$H_2S + H \longrightarrow HS + H_2 \qquad \text{[R1]}$$
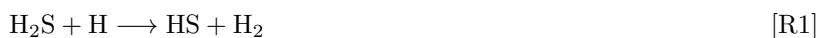
The resulting HS radical quickly reacts to free sulfur and form S_2

$$HS + H \longrightarrow S + H_2 \qquad\qquad [R2]$$

$$HS + S \longrightarrow H + S_2 \qquad\qquad [R3]$$
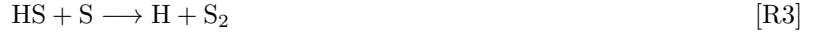
This begins the polymerization process to form higher sulfur allotropes, eventually creating the stable allotrope, S_8. Transport of S_8 into the deep atmosphere then results in its destruction via thermal decomposition

$$S_8 + M \longrightarrow 2S_4 + M \qquad\qquad [R4]$$

the products of which go on to decompose further before reforming H_2S, thus completing the cycle. In the event that the equilibrium S_8 partial pressure is above the saturation vapor pressure P_{sat} of S_8 somewhere in the atmosphere, given by

$$P_{sat} = \begin{cases} \exp\left(20 - 11800/T\right) & T < 413\text{K} \\ \exp\left(9.6 - 7510/T\right) & T > 413\text{K} \end{cases} \qquad (1)$$
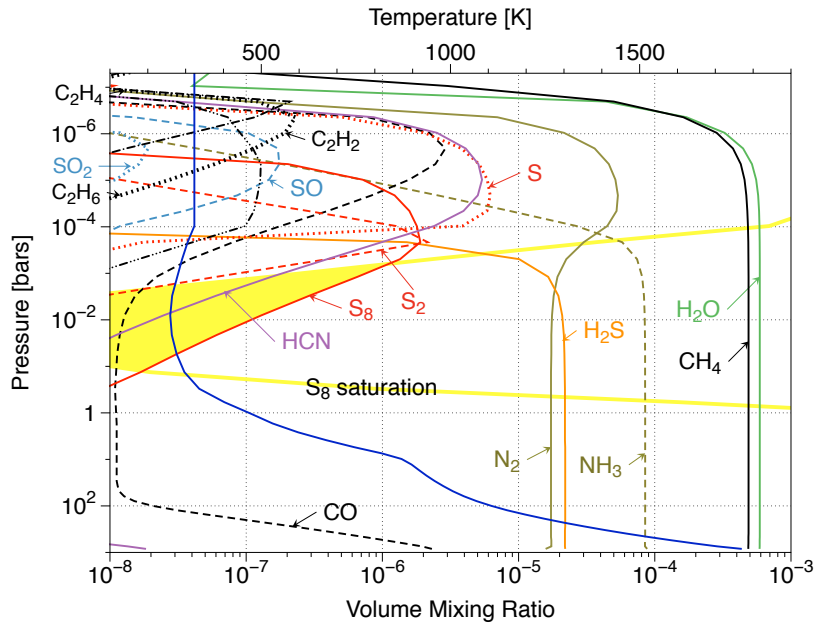
then an S_8 haze may form.

Figure 1. The temperature profile (blue), S_8 saturation vapor mixing ratio (yellow), and equilibrium mixing ratios of several important and/or sulfur–derived chemical species in a model giant exoplanet atmosphere subject to photochemistry and eddy diffusion. The shaded yellow region indicates where S_8 is supersaturated.

Figure 1 shows the temperature profile (blue), saturation mixing ratio of S_8 (saturation vapor pressure divided by total atmospheric pressure, in yellow), and the equilibrium mixing ratios of numerous chemical species in a temperate giant exoplanet atmosphere (see §3.1) as a result of photochemistry and transport by eddy diffusion. The equilibrium mixing ratio of S_8 peaks at ∼1 ppmv, and crosses the S_8 saturation mixing ratio curve between 100 and 1 mbar (the yellow region). This allows for a rough estimate of the total mass of the haze, assuming that all S_8 that is supersaturated condenses. For example, 1 ppmv of S_8 at the 100 mbar level with $T \sim 250$ K results in a number density of S_8 molecules of $\sim 3 \times 10^{12}$ cm^{-3}. Assuming a column height equaling one scale height (∼20 km at 100 mbar

for this atmosphere), then the column integrated number density of S_8 is $\sim 6 \times 10^{18}$ cm^{-2}, which translates to a haze particle column number density of $\sim 3 \times 10^{11}$ cm^{-2} assuming a particle size of 0.1 μm and a mass density of 2 g cm^{-3}.

The ultimate haze mass will depend on the degree to which S_8 is supersaturated, which in turn depends on the equilibrium S_8 mixing ratio and the S_8 saturation vapor mixing ratio. Zahnle et al. (2016) showed that, for a wide range in stellar UV fluxes and eddy diffusivities, the peak equilibrium S_8 mixing ratio remained close to 1 ppmv to within a factor of 2, though its vertical profile became more extended/compressed when the eddy diffusivity increased/decreased, respectively. The S_8 mixing ratio is largely independent of stellar UV fluxes because the fluxes experienced by temperate giant exoplanets are such that the photochemistry is limited by H_2S upwelling, rather than the supply of UV photons. The S_8 mixing ratio is also independent of the eddy diffusivity because, in the event that S_8 does not condense, the upward mixing of H_2S is balanced by the downward mixing of S_8, and thus changing the rate of mixing should not change the size of the reservoirs from which material is exchanged by mixing. Furthermore, as Figure 1 shows, changing the temperature does not alter the S_8 mixing ratio a large degree either. This likely results from the stability of S_8, such that it can act as an ultimate sink for sulfur above the region where it thermally decomposes. In other words, though varying the temperature changes the rates of reactions, all reactions eventually lead to the transformation of H_2S to S_8 above the tropopause.
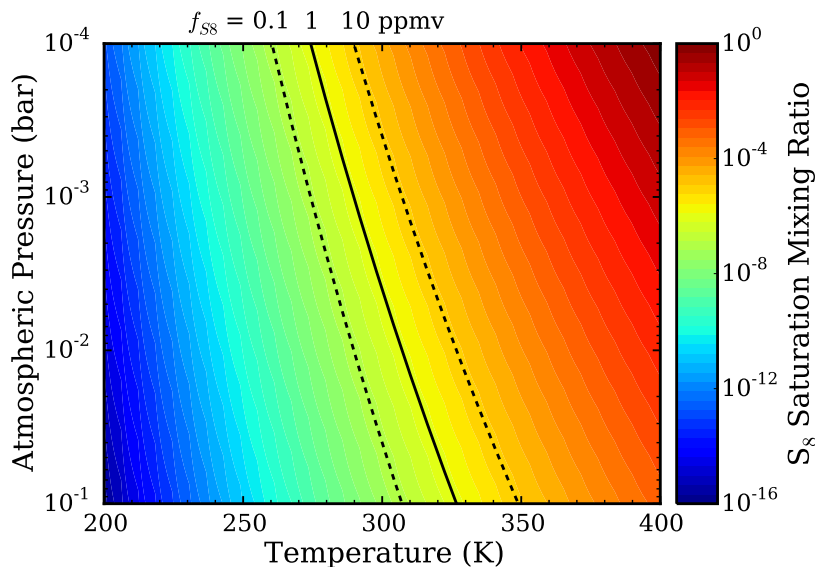

Figure 2. S_8 saturation vapor mixing ratio as a function of temperature and background atmospheric pressure. The solid line indicates where the S_8 saturation vapor mixing ratio equals 1 ppmv, while the dotted lines to the left and right indicate 0.1 and 10 ppmv, respectively.

Given the stability of the equilibrium S_8 mixing ratio, the haze mass will largely depend on the saturation vapor mixing ratio, which is a function of temperature. Figure 2 shows the S_8 saturation vapor mixing ratio as a function of temperature and pressure level in the atmosphere, where the range in pressure level denotes where S_8 tends to be abundant (Zahnle et al. 2016). The solid line indicates a saturation vapor mixing ratio of 1 ppmv, while the dashed lines to the left and right side of it indicate 0.1 and 10 ppmv, respectively. Thus, if an exoplanet atmosphere contains 1 ppmv of S_8 , then condensation can occur (S_8 is supersaturated) for temperatures and atmospheric pressure levels to the left of the 1 ppmv line, while to the right the abundance of S_8 is too low to condense. A complication arises at low temperatures however, due to the condensation of NH_3, which reacts with H_2S to form NH_4SH clouds. This process has been hypothesized to occur in the atmospheres of Jupiter and Saturn (e.g. Atreya et al. 1999). Once H_2S is lost to NH_4SH it will no longer be available as a sulfur source to photochemically form S_8. Therefore, we can conclude that sulfur hazes may arise on temperate giant exoplanets with stratospheric temperatures <325K but warmer than Jupiter, given that their metallicity is solar. Increased metallicity leads to a wider temperature range in which sulfur can condense, and vice versa for lower metallicity.

The effect of a sulfur haze on a planet's geometric albedo depends heavily on sulfur's optical properties, stemming primarily from its complex refractive index. Figure 3 shows the real (n) and imaginary (k) indices of refraction
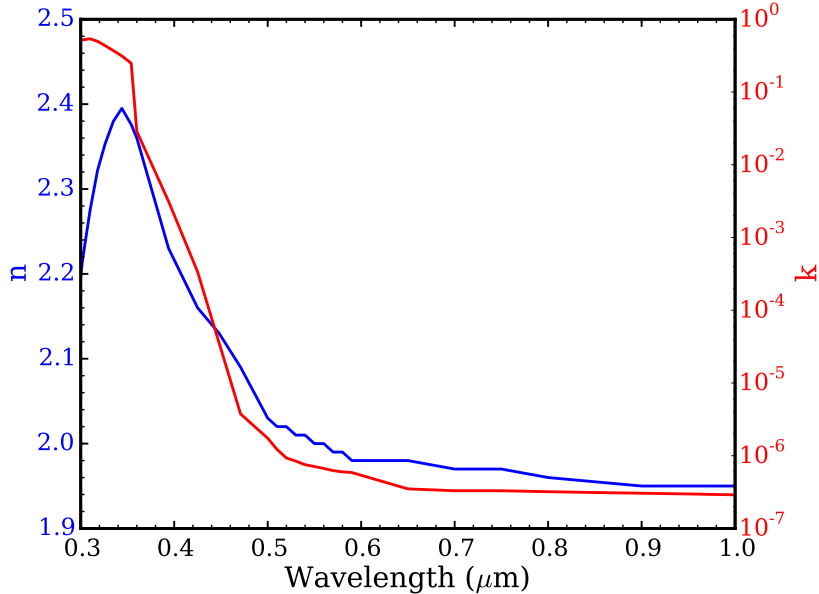
Figure 3. Real (blue) and imaginary (red) components of S_8's complex refractive index (Fuller et al. 1998)

for orthorhombic crystals of sulfur, a form of solid sulfur composed mainly of S_8. Orthorhombic sulfur is the most stable form of solid sulfur for the temperatures relevant here, though an alternative form, monoclinic sulfur, exists transiently with conversion rates to orthorhombic sulfur decreasing with decreasing temperature (Fuller et al. 1998), though conversion of orthorhombic sulfur to monoclinic sulfur becomes preferred above 368 K (Meyer 1976). A key feature of orthorhombic sulfur's complex refractive index is the increase in k at shorter wavelengths caused by vibrational modes in the S_8 molecules, which tend to become more populated at higher temperatures, thereby shifting the increase in k to longer wavelengths (Meyer et al. 1972). Increased absorption at shorter wavelengths will lead to sulfur haze–enveloped exoplanets being yellowish to reddish in color.

3. METHODS

3.1. *Model Atmosphere*

We evaluate the effect a sulfur haze would have on a planet's geometric albedo spectrum by introducing a sulfur haze into a 1–dimensional model background atmosphere, which we initially assume to be devoid of clouds or hazes. The pressure–temperature profile of the model atmosphere is set by asserting radiative–convective equilibrium, and its molecular composition is determined by assuming thermochemical equilibrium. The planetary parameters are chosen to be that of Gamma Cephei Ab, a warm giant exoplanet discovered via radial velocities (Campbell et al. 1988; Hatzes et al. 2003) with a minimum mass of 1.85 Jupiter masses, and which orbits its host star, a K1IVe subgiant with an effective temperature of 4800 K and a stellar radius of 4.9 solar radii, at a semimajor axis of 2.05 AU (Torres 2007; Endl et al. 2011). Figure 1 shows the model atmosphere pressure–temperature profile in blue, where only the regions below 0.1 mbar are in radiative–convective equilibrium, with the radiative/convective boundary at ∼0.1 bar. Extension of the PT profile upwards was necessary to investigate the abundance of S_8 produced in this model atmosphere due to photochemistry, but we do not consider the regions above 0.1 mbar in our geometric albedo calculations. We chose Gamma Cephei Ab due to its moderate stratospheric temperatures, which could be conducive to sulfur haze formation.

The PT profile of our atmosphere is generated using the iterative radiative–convective model developed in McKay et al. (1989), and extended by Marley et al. (1996); Marley & McKay (1999); Marley et al. (2002); Burrows et al. (1997); Fortney et al. (2005, 2008); Saumon & Marley (2008). Given an internal heat flux and incident flux from the host star, the PT profile is adjusted until (1) the net flux between the plane–parallel atmospheric layers is zero and (2) the profile adheres to convective stability. The radiative transfer is treated via the two–stream source function method described in Toon et al. (1989), with opacities of molecular species provided by Freedman et al. (2008) with updates from Saumon et al. (2012) and combined using the correlated–k method (Goody et al. 1989).

We assume solar metallicity for the model atmosphere (Lodders 2003), and calculate its molecular composition by minimizing the Gibbs free energy to ensure thermochemical equilibrium. The major chemical species that are abundant and/or optically active include H_2, H, VO, TiO, CO_2, He, H2O, CH_4, CO, NH_3, N_2, PH_3, H_2S, Fe, Na, and K. In

the event that a species becomes supersaturated, it is assumed to be depleted via condensation above the crossing point between its partial pressure and its saturation vapor pressure (Lodders 1999). The thermochemical equilibrium composition is used to calculate the planet's geometric albedo, and serve as initial conditions for the time–stepping photochemical model, the results of which are shown in Figure 1.

3.2. Cloud Model and Haze Treatment

The PT profile of our model atmosphere is such that KCl and ZnS can potentially condense and form clouds (Morley et al. 2012). To include clouds in our model we use the approach of Ackerman & Marley (2001), where the cloud mass and mean particle size is determined by balancing vertical mixing due to eddy diffusion and sedimentation of cloud particles

$$K_{zz} \frac{\partial q_{\mathrm{t}}}{\partial z} + f_{\mathrm{sed}} w q_{\mathrm{c}} = 0 \tag{2}$$

where q_t is the total mixing ratio of the condensing species, q_c is the mixing ratio of the condensed form of the condensing species only, w is the convective velocity, f_{sed} is a tunable parameter and a measure of the sedimentation efficiency of the cloud particles that we set to 3, appropriate for Jupiter–like words (Ackerman & Marley 2001; Saumon & Marley 2008; Morley et al. 2012), and K_{zz} is the eddy diffusion coefficient, calculated by assuming that the convective mass transport is equivalent to convective heat transport. A minimum value $K_{zz}^{min} = 10^5$ cm^2 s^{-1} is set in regions that are convectively stable, as eddy diffusion does not only represent convective turbulence. w is then calculated via mixing length theory: $w = K_{zz}/L$, where L is the mixing length given by

$$L = H \max(0.1, \Gamma/\Gamma_{ad}) \tag{3}$$

where H is the atmospheric scale height, Γ and Γ_{ad} are the local and dry adiabatic lapse rates, and 0.1 is the minimum scaling for L when the atmosphere is convectively stable.

For both the clouds and sulfur haze, we assume that the particle size distribution dn/dr is lognormal, given by

$$\frac{dn}{dr} = \frac{N}{r\sqrt{2\pi}\ln\sigma} \exp\left[-\frac{\ln^2\left(r/r_g\right)}{2\ln^2\sigma}\right] \tag{4}$$

where N is the total number density of particles, r is the particle radius, and σ is a measure of the width of the distribution and is fixed to 2 in the cloud model.

While the Ackerman & Marley (2001) model is appropriate for clouds that are supported by vertical mixing, it cannot be used to simulate photochemical hazes that have an in situ source. Therefore, we prescribe a sulfur haze with a set location in the atmosphere, particle number density, and mean particle radius. We position our nominal sulfur haze layer at the 10 mbar level in the model atmosphere, consistent with the results of Zahnle et al. (2016) and our Figure 1; the column number density of the haze is set to 10^{11} cm^{-2}, in agreement with our calculations of the haze mass in §2; and the mean particle radius is set to 0.1 μm, similar to mode 1 particles in the clouds of Venus, which may be composed of elemental sulfur (Knollenberg & Hunten 1980).

The optical properties of the clouds and the sulfur haze, such as their optical depth, single scattering albedo, and asymmetry parameter (a measure of their degree of forward scattering) are calculated by the cloud model using Mie theory assuming homogeneous spheres. As with the sulfur haze, the optical properties of the clouds are determined by their complex indices of refraction, which for KCl and ZnS are provided by Querry (1987).

In a self–consistent atmosphere, the formation of clouds and hazes would perturb the PT profile, which will in turn lead to different molecular abundances. However, for this exercise we do not ensure this self-consistency. Instead, the PT profile is fixed to that of a clear atmosphere (though the molecular abundances do reflect condensation), with condensate clouds and the prescribed sulfur haze layer added to it afterwards. We discuss the consequences of this assumption in §5.

3.3. Geometric Albedo Model

The geometric albedo of a planet is defined as the ratio of the reflected flux of that planet at full phase to the reflected flux from a perfect Lambert disk with the same radius as the planet located at the same distance from its host star (Cahoy et al. 2010). The reflecting hemisphere of our cloudy/hazy planet is split into individual 1–dimensional atmospheric columns with plane–parallel layers, and radiative transfer calculations for each column is performed separately following Toon et al. (1989), relating incident fluxes to reflected fluxes. At full phase, each patch

on the planet has the same observer and solar zenith angle, and these vary across the disk due to the curvature of the reflecting hemisphere. The geometric albedo spectrum is then calculated by averaging over the reflected flux from each column weighted by viewing geometry at full phase (Cahoy et al. 2010).

Opacity sources considered when calculating the geometric albedo spectrum include molecular absorption as previously mentioned (including collision–induced absorption of H_2–H, H_2–H_2, H_2–He, and H_2–CH_4), as well as Rayleigh scattering (Cahoy et al. 2010) and Raman scattering (Pollack et al. 1986). The optical depths, single scattering albedos, and asymmetry parameters calculated by the cloud model are used to account for the opacity of the condensate clouds and the sulfur haze.

3.4. *WFIRST Noise Model*

WFIRST (Wide Field Infrared Survey Telescope) is a planned NASA mission to be launched in the mid–2020s. It is a space–based, coronagraph–equipped observational platform with a 2.4 m diameter primary aperture, an operational wavelength range from ∼0.4 to 1 μm, and a spectral resolution of 70 (Spergel et al. 2013). Robinson et al. (2016) showed, using a state–of–the–art noise model, that given a coronagraph capable of achieving a planet–star contrast ratio of 10^{-9} and expected levels of read noise, dark current, leaked stellar light, and zodiacal light from the Solar System and the exoplanetary system, a giant exoplanet located at 2 AU from a sun–like star is readily detectable and characterizable with integration times of several tens of hours, provided that the exoplanetary system is located within about 10 pc and that the planet–star angular separation is within the coronagraph inner and outer working angles.

We investigate the observability of a sulfur haze using an updated version of this noise model, which includes specific coronagraph designs that have been proposed for WFIRST, such as the Shaped–Pupil Coronagraph (SPC; capable of both broadband imaging and spectroscopy; Kasdin et al. 2004) and the Hybrid Lyot Coronagraph (HLC; imaging mode only; Trauger et al. 2016). The baseline telescope and instrument parameter values corresponding to these coronagraphs are different from that of Robinson et al. (2016) (see their Table 3). We show these updated values in Table 1.

Table 1. Old and Updated Baseline Telescope and Instrument Parameter Values

Parameter	Description	Old Value	Updated Value (HLC)	Updated Value (SPC)
D	telescope diameter	2 m	2.4 m	2.4 m
R_{e-}	read noise counts per pixel	0.1	0.2	0.2
$\mathcal{T}$	telescope and instrument throughput	0.05	0.074	0.037
θ_{IWA} (λ/D)	coronagraph inner working angle	2	2.8	2.7

NOTE—Only updated parameters are shown.

To use the noise model, we position our exoplanetary system, composed of the K1IVe subgiant host star and the warm giant exoplanet at 8 pc so that the full wavelength range under consideration can be observed without going beyond the inner or outer working angles (the real Gamma Cephei Ab is located 13.79 pc away (Hatzes et al. 2003), such that wavelengths longer than ∼0.6 μm would not be observable due to the planet–star on–sky separation for those wavelengths being within WFIRST's inner working angle). In addition, we assume that (1) the exozodi brightness is the same as zodiacal light in our own Solar System and (2) our model planet has the same radius as Jupiter. As the observation would likely be made while the exoplanet is at quadrature rather than at full phase, we multiply the contrast ratio calculated from the (full phase) geometric albedo by a correction factor $1/\pi$, roughly simulating the drop in brightness at quadrature versus full phase. However, this does not take into account the changes in geometric albedo due to non–uniform scattering phase functions of the clouds and hazes in the atmosphere. It should also be noted that the real Gamma Cephei A is part of a binary system, which would reduce WFIRST's ability to reach its designed planet–star raw contrasts. For simplicity, we assume that our model host star does not have a stellar companion.

4. RESULTS

Figure 4 shows the geometric albedo spectra of a clear Gamma Cephei Ab atmosphere (black), an atmosphere with KCl and ZnS clouds included (blue), and our nominal hazy model including both the aforementioned clouds and a
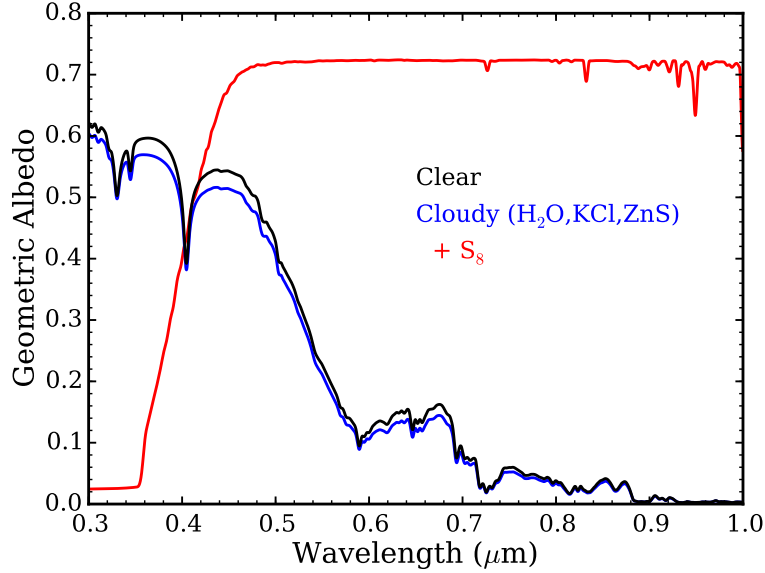
Figure 4. Geometric albedo spectra for a clear (black), cloudy (blue), and hazy (red) giant exoplanet atmosphere. The cloudy case includes KCl and ZnS clouds. The hazy case includes all aforementioned clouds, and the nominal sulfur haze layer located at 10 mbar with a column number density of 10^{11} cm^{-2} and a mean particle size of 0.1 μm.

sulfur haze (red). Absorption features due to H_2O and CH_4 can be clearly discerned at longer wavelengths in the clear case, which makes the planet especially dark there. At shorter wavelengths Rayleigh scattering increases the geometric albedo, with absorption dominated by alkali metals such as potassium (Cahoy et al. 2010). Adding condensation clouds does not change the geometric albedo significantly, as the metallicity is not high enough to produce optically thick KCl and ZnS clouds. The resulting cloudy geometric albedo spectrum is simply less bright than the clear case due to decreased Rayleigh scattering caused by decreased path lengths for photons in the atmosphere resulting from the presence of diminutive KCl and ZnS clouds.

In contrast, adding a sulfur haze layer drastically alters the geometric albedo spectrum. The CH_4 and H_2O absorption bands are now mostly absent save for some small dips longward of 0.7 μm, where the planet is much brighter due to the purely scattering sulfur haze there, while at wavelengths <0.45 μm the albedo drops precipitously due to increased sulfur absorption. These features are the exact opposite of the clear case, where the planet is darker at long wavelengths and bright at short wavelengths. The shape of the geometric albedo spectrum also contrasts with those produced by hazes composed of other materials. Soots, for example, darken the planet across the entire wavelengths range studied here, while tholins are more similar to sulfur in that it also brightens a planet at long wavelengths while darkening it short wavelengths, though the transition from high to low albedo for a tholin haze is considerably more gradual (Morley et al. 2015).

Figure 5 shows the variations in the geometric albedo spectrum as the sulfur haze layer is placed at different pressure levels, within the range of pressure levels where S_8 is abundant. The location of the sulfur haze layer can be variable since it depends on where the S_8 mixing ratio curve intercepts the S_8 saturation vapor mixing ratio curve, which in turn is a function of the atmospheric temperature structure and intensity of vertical mixing. There is very little difference between the different cases, with the only variations due to increased absorption by CH_4 and H_2O as the haze is lowered in the atmosphere, thereby increasing the optical depth of these gases above the haze.

Figure 6 shows the changes in the geometric albedo spectrum as the column number density of sulfur haze particles is varied. The column number density is strongly related to the degree of supersaturation of S_8 vapor and is controlled largely by the microphysics of sulfur haze formation. Increasing the column number density from our nominal case does not change the geometric albedo spectrum to any large degree, indicating that the effect of the sulfur haze has already "saturated" for our nominal haze abundance. This is not surprising since the optical depth of our nominal case is already >1. Decreasing the column number density past an optical depth of 1 reduces the effect of the haze on the geometric albedo. In particular, the brightness of the planet is reduced significantly longward of 0.45 μm until it begins to match the clear case. By contrast, the geometric albedo shortward of 0.45 μm remains largely unchanged even at very low sulfur haze optical depths, only approaching the clear case for optical depths 1000 times less than
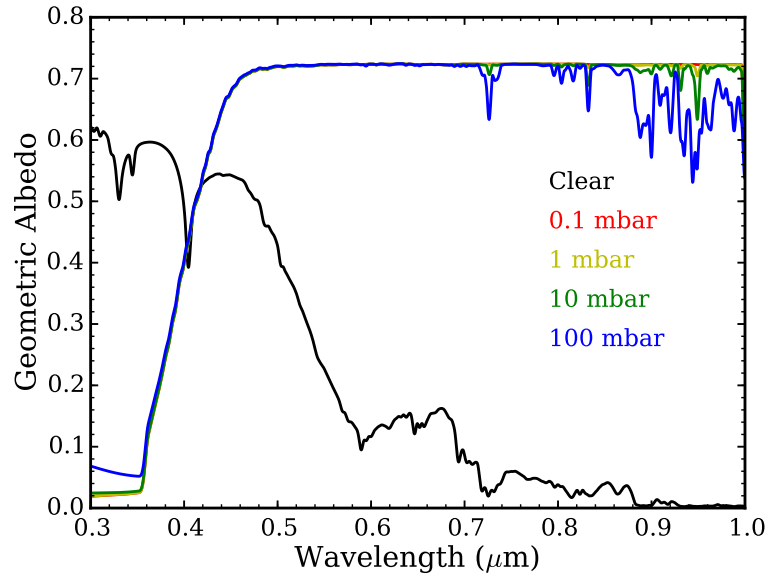
Figure 5. Geometric albedo of a giant exoplanet with a sulfur haze located at 0.1 (red), 1 (yellow), 10 (green), and 100 mbar (blue). The geometric albedo of a clear atmosphere (black) is shown for comparison.
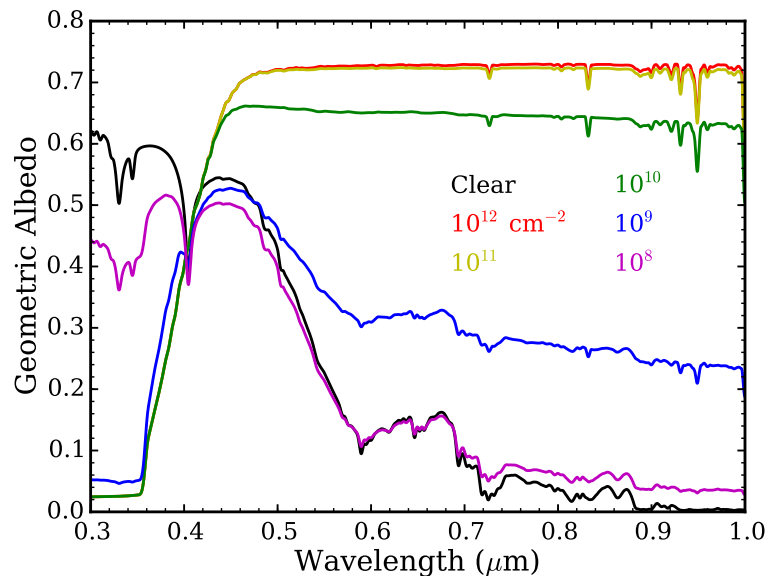

Figure 6. Geometric albedo of a giant exoplanet with a sulfur haze with column number densities of 10^{12} (red), 10^{11} (yellow), 10^{10} (green), 10^9 (blue), and 10^8 cm^{-2} (magenta). The geometric albedo of a clear atmosphere (black) is shown for comparison.

that of the nominal case.

Figure 7 shows the changes in the geometric albedo spectrum as the mean sulfur haze particle size is varied, while keeping the total haze mass the same (i.e. increasing particle size leads to a lower column number density). Like the column number density, the particle size depends on the microphysics of sulfur haze formation and growth by condensation of S_8 vapor. Varying the particle size is seen to have different effects depending on whether the particles are mostly scattering (longward of 0.45 μm) or absorbing (shortward of 0.45 μm). In the scattering region, decreasing the particle size such that it becomes much smaller than the wavelength results in a Rayleigh slope developing at longer wavelengths, darkening the planet slightly. Increasing the particle size past the considered wavelength range leads to a decrease in the geometric albedo due to the decrease in haze optical depth. This results from the consolidation of haze mass in larger particles, since optical depth is proportional to the square of the particle radius, while particle mass
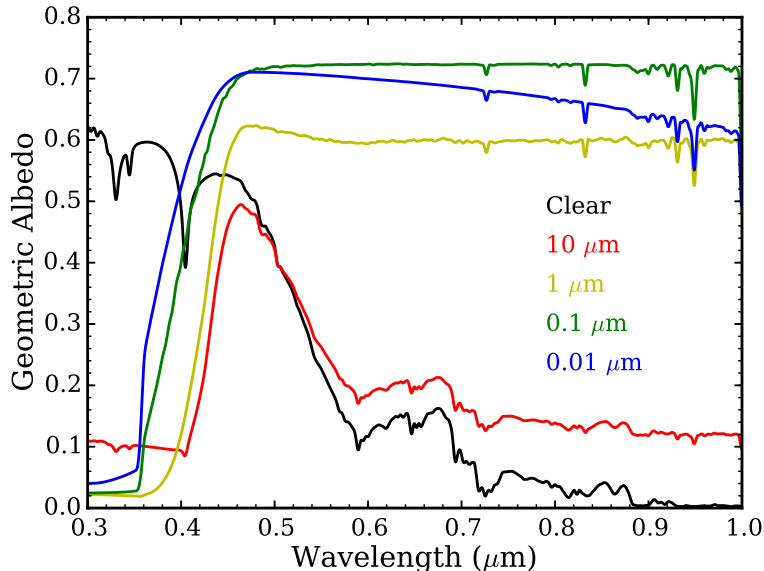
Figure 7. Geometric albedo of a giant exoplanet with a sulfur haze with a mean particle radius of 0.01 (red), 0.1 (yellow), 1 (green), and 10 μm (blue). The total haze mass is kept constant for cases. The geometric albedo of a clear atmosphere (black) is shown for comparison.

is proportional to the cube of the particle radius, and the scattering efficiency is largely independent of the particle radius for radii much greater than the wavelength (van de Hulst 1957). The geometric albedo is largely unchanged in the absorbing part of the spectrum. This can be explained by the roughly linear relationship between particle size and the absorption efficiency (van de Hulst 1957); in other words, the decrease in haze optical depth due to consolidating mass in larger particles is balanced by an increase in absorption by those larger particles. In addition, the wavelength at which the geometric albedo drops abruptly moves to longer wavelengths with increasing particle size. This is caused by the increasing importance of absorption for larger particles, and also that the smallest particles are more Rayleigh scattering, thereby increasing the albedo at shorter wavelengths.

Using the WFIRST noise model from Robinson et al. (2016), we can assess whether the drastic changes to a giant exoplanet's geometric albedo caused by a sulfur haze layer is detectable. Figure 8 shows the low resolution (R = 70) planet–star flux ratio multiplied by 10^9 for the clear atmosphere case (blue) and the nominal hazy case (red). Superimposed on the spectra are synthetic observations taken by the shaped pupil coronagraph (SPC) in imaging (black) and spectroscopy (gray) mode, and the hybrid Lyot coronagraph (HLC; magenta), each with a 20 hour integration time per observation. Note that the shaped pupil coronagraph in spectroscopy mode requires three exposures to capture its full wavelength range, so the full observation time to obtain SPC spectra is 60 hours.

There is a significant difference between the clear and hazy cases. For the wavelength range WFIRST is able to observe, the hazy planet is brighter by a factor of ∼6, and thus easier to detect. On the other hand, the minor CH_4 and H_2O absorption features in the hazy spectra are not detectable, thus rendering any effort to retrieve their abundances hopeless (Lupu et al. 2016). With the added HLC channel at 0.465 μm, a Rayleigh slope is discernible in the clear case, whereas the hazy case is flat for all observable wavelengths, making clear and hazy atmospheres easily distinguishable. However, the flat spectrum of the hazy case could also be interpreted as due to high water ice clouds in a colder atmosphere (Morley et al. 2015), making it difficult to confirm that the high albedo is indeed caused by a sulfur haze.

5. DISCUSSION

We have shown that the existence of a sulfur haze can significantly alter the geometric albedo spectrum of a temperate giant exoplanet. However, our results depend greatly on the properties of the haze, such as the mean particle size and column number density, both of which are determined by microphysical processes, such as nucleation of aerosols, growth by condensation and coagulation, loss through evaporation and collisional breakup, and transport by sedimentation, mixing, and advection (Pruppacher & Klett 1978; Marley et al. 1999). Although the modeling of these processes is beyond the scope of this work and will be treated in a future paper, we can speculate on how a sulfur haze subject to microphysics differ from the simple slab model we have used. A major difference would be the vertical profile of the
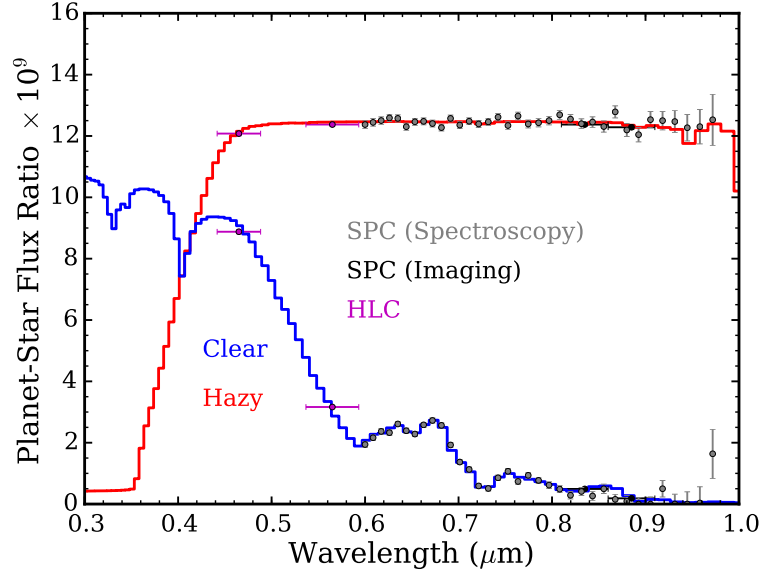
Figure 8. Planet–star flux ratio $\times 10^9$ for a clear (blue) and hazy (red) giant exoplanet with a radius of 1 Jupiter radii, located 8 pc away, and orbiting a K1IVe subgiant with a radius of 4.9x solar radii and an effective temperature of 4800 K at 2.05 AU. Synthetic data from the shaped pupil coronagraph (SPC) in imaging (black) and spectroscopy (gray) mode and the hybrid Lyot coronagraph (HLC; magenta), possible instruments onboard WFIRST, are overplotted. Integration time for each exposure is set to 20 hours, with the SPC in spectroscopy mode needing 3 exposure to cover the full wavelength range presented in the figure.

haze. Vertical mixing will loft sulfur particles to higher altitudes, where the lower atmospheric pressure and S_8 mixing ratio may result in evaporation of haze particles and a decrease in mean particle size. A haze layer with a vertical gradient in mean particle size would generate a different geometric albedo spectrum than a layer with the same size distribution at all altitudes.

Given that the sulfur haze would have a source of new particles at or near the altitude where S_8 is photochemically produced, there exists the possibility of multi–modal particle size distributions. The situation is similar to that of Venus, where large, ~ 1 μm sulfuric acid cloud particles coexist with ~ 0.1 μm particles of photochemical origins, possibly composed of elemental sulfur or sulfuric acid as well (e.g. Knollenberg & Hunten 1980; Imamura & Hashimoto 2001; Gao et al. 2014). In our case, freshly nucleated sulfur haze particles may coexist with larger, "aged" sulfur particles that have grown by the condensation of S_8 and other sulfur allotropes, resulting in more complex geometric albedo spectra than those presented here.

In addition to the microphysics of the haze itself, the effect of the haze on the rest of the atmosphere must be considered. The chemical abundances presented in Figure 1 does not take condensation into account. Indeed, if S_8 condenses then all other sulfur allotropes may condense on the S_8 particles as well, as their saturation vapor pressures are all significantly lower (Lyons 2008; Zahnle et al. 2016). This will have the effect of not only changing the sulfur chemistry in the atmosphere, possibly removing all sulfur species above the haze layer, but also introduce/increase contamination of the haze particles by smaller sulfur allotropes such as the metastable S_3 and S_4, thereby changing the optical properties of the haze and its geometric albedo spectrum (Meyer et al. 1972). Furthermore, as H_2S is key in forming sulfide clouds in exoplanet atmospheres (Morley et al. 2012), including the ZnS clouds in our model, and sulfur haze particles can potentially form condensation nuclei for cloud formation, perturbations to the sulfur chemistry and emergence of sulfur hazes could impact condensation clouds as well.

The strong absorption of UV photons by sulfur hazes is also likely to affect the rest of the atmosphere. On Venus, absorption of UV by an unknown agent in the mesosphere, possibly sulfur (Mills et al. 2007), leads to several K day^{-1} of heating (Crisp 1986; Haus et al. 2015, 2016). Such heating in a giant exoplanet atmosphere may increase temperatures, affecting the sulfur haze abundance. Increasing the haze temperature also increases the wavelength of sulfur's UV absorption edge, though the change is small over the temperature range of relevance (~ 0.23 nm K^{-1}; Meyer et al. 1972). Calculating the equilibrium temperature profile due to haze heating will require a more sophisticated model.

The current configuration of WFIRST cannot observe the strong absorption of sulfur hazes shortward of 0.45 μm,

which is its defining feature between 0.3 and 1 μm. Future telescopes capable of direct imaging, such as the LUVOIR or HabEx mission concepts, could potentially probe down to such short wavelengths. Alternatively, sulfur hazes may be discernible by JWST in the infrared. The compilation of orthorhombic sulfur complex refractive indices provided by Fuller et al. (1998) show a gap in the imaginary component between 2 and 7 μm, likely indicating that it was too low to be measured precisely; beyond 7 μm, k increases steadily from 10^{-6} to 10^{-2} with punctuating spikes up to as high as 0.1. We will investigate JWST's capabilities for characterizing sulfur hazes in a future publication.

We have demonstrated that sulfur photochemistry in temperate giant exoplanets with solar metallicity inexorably generates $\sim$1 ppmv of S_8 vapor for large swaths of planetary parameter space. Therefore, a sulfur haze could form if the stratospheric temperature is low enough such that S_8 becomes supersaturated. The effect of such a sulfur haze on the planet's geometric albedo is significant: pure scattering sulfur particles boost the albedo longward of 0.45 μm to $\sim$0.7, while strong absorption shortward of 0.45 μm lowers the albedo to near zero. This is the opposite trend to a clear atmosphere, where deep molecular absorption darkens a planet at long wavelengths while Rayleigh scattering brightens the planet at short wavelengths.

The impact of the sulfur haze on the geometric albedo is largely independent of where the haze is located in the atmosphere within the range where S_8 vapor is abundant, though CH_4 and H_2O bands do become slightly more pronounced as the haze is placed deeper into the atmosphere. In contrast, changing the optical depth of the haze by varying the particle column number density or the mean particle size does drastically change the resulting geometric albedo spectrum, though the absorption at short wavelengths remains robust even at optical depths 1/1000th that of our nominal case. Physically constraining the optical depth of sulfur hazes will require more detailed, coupled photochemical–microphysical models that feedback on the atmospheric thermal structure due to sulfur haze UV heating.

Sulfur hazes on temperate giant exoplanets may be detectable by the next generation of space–based observatories like WFIRST, though discriminating whether the high albedo is caused by sulfur or by other reflective materials (e.g. water ice) will require wavelength coverage shortward of the absorption edge at 0.45 μm, which is not currently planned for WFIRST. In addition, extracting the abundances of CH_4 and H_2O of such planets from WFIRST observations may be difficult due to the haze, and will likely require further observations at different wavelengths.

REFERENCES

Ackerman A. S. & Marley, M. S. 2001, ApJ, 556, 872

Atreya, S. K., Wong, M. H., Owen, T. C., et al. 1999, Planet. Space Sci., 47, 1243

Beichman, C., Benneke, B., Knutson, H. A., et al. 2014, PASP, 126, 1134

Burrows, A., Marley, M. S., Hubbard, W. B., et al. 1997, ApJ, 491, 856

Cahoy, K. L., Marley, M. S., & Fortney, J. J. 2010, ApJ, 724, 189

Campbell, B., Walker, G. A. H., & Yang, S. 1988, ApJ, 331, 902

Chen, G., van Boekel, R., Wang, H., et al. 2014, A&A, 563, A40

Crisp, D. 1986, Icarus, 67, 484

Crossfield, I. J. M., Barman, T., Hansen, B. M. S., et al. 2013, A&A, 559, A33

Deming, D., Wilkins, A. N., McCullough, P., et al. 2013, ApJ, 774, 95

Endl, M., Cochan, W. D., Hatzes, A. P., et al. 2011, arXiv:1101.2588

Fortney, J. J., Marley, M. S., Lodders, K., et al. 2005, ApJL, 627, L69

Fortney, J. J., Marley, M. S., Saumon, D., et al. 2008, ApJ, 683, 1104

Freedman, R. S., Marley, M. S. & Lodders, K. 2008, ApJS, 174, 504

Fukui, A., Kawashima, Y., Ikoma, M., et al. 2014, ApJ, 790, 108

Fuller, K. A., Downing, H. D., & Querry, M. R. 1998, Orthorhombic Sulfur (α–S), In: Handbook of Optical Constants of Solids III, Ed. Palik, E. D. (San Diego, Academic Press)

Gao, P., Zhang, X., Crisp, D., et al. 2014, Icarus, 231, 83

Gibson, N. P., Aigrain, S., Pont, F., et al. 2012, MNRAS, 422, 753

Gibson, N. P., Aigrain, S., Barstow, J. K., et al. 2013, MNRAS, 428, 3680

Goody, R., West, R., Chen, L., et al. 1989, J. Quant. Spectrosc. Radiat. Transfer, 42, 539

Hansen, J. E. & Hovenier, J. W. 1974, J. Atmos. Sci., 31, 1137

Hatzes, A. P., Cochran, W. D., Endl, M., et al. 2003, ApJ, 599, 1383

Haus, R., Kappel, D., & Arnold, G. 2015, Planet. Space Sci., 117, 262

Haus, R., Kappel, D., & Tellmann, S. 2016, Icarus, 272, 178

Hu, R., Seager, S., & Bains, W. 2013, ApJ, 769, 6

Imamura T. & Hashimoto, G. L. 2001, J. Atmos. Sci., 58, 3597

Jordán, A., Espinoza, N., Rabus, M., et al. 2013, ApJ, 778, 184

Junge, C. E. 1963, J. Geophys. Res., 68, 3975

Kasdin, N. J., Vanderbei, R. J., Littman, M. G., et al. 2004, Proc. SPIE, 5487, 1312

Khare, B. N., Sagan, C., Arakawa, E. T., et al. 1984, Icarus, 60, 127

Knollenberg R. G. & Hunten, D. M. 1980, J. Geophys. Res., 85, 8039

Knutson, H. A., Benneke, B., Deming, D., et al. 2014, Nature, 505, 66

Knutson, H. A., Dragomir, D., Kreidberg, L., et al. 2014, ApJ, 794, 155

Kreidberg, L., Bean, J. L., Désert, J.–M., et al. 2014, Nature, 505, 69

Lodders, K. 1999, ApJ, 519, 793

Lodders, K. 2003, ApJ, 591, 1220

Lupu, R. E., Marley, M. S., Lewis, N., et al. 2016, arXiv:1604.05370

Lyons, J. R. 2008, J. Sulfur Chem., 29, 269

Mallonn, M. & Strassmeier, K. G. 2016, A&A, 590, A100

Mandell, A. M., Haynes, K., Sinukoff, E., et al. 2013, ApJ, 779, 128

Marley, M. S., Saumon, D., Guillot, T., et al. 1996, Science, 272, 1919

Marley, M. S. & McKay, C. P. 1999, Icarus, 138, 268

Marley, M. S., Gelino, C., Stephens, D., et al. 1999, ApJ, 513, 879

Marley, M. S., Seager, S., Saumon, D., et al. 2002, ApJ, 568, 335

McKay, C. P., Pollack, J. B., & Courtin, R. 1989, Icarus, 80, 23

Meyer, B., Gouterman, M., Jensen, D., et al. 1972, The Spectrum of Sulfur and its Allotropes, In: Sulfur Research Trends, Eds. Miller, D. J. & Wiewiorowski, T. K. (Washington, D. C., American Chemical Society Publishing)

Meyer, B. 1976, Chem. Rev., 76, 367

Mills, F. P., Esposito, L. W., & Yung, Y. L. 2007, Atmospheric Composition, Chemistry, and Clouds, In: Exploring Venus as a Terrestrial Planet, Eds. Esposito, L. W., Stofan, E. R., & Cravens, T. E. (Washington, D. C., American Geophysical Union)

Morley, C. V., Fortney, J. J., Marley, M. S., et al. 2012 ApJ, 756, 172

Morley, C. V., Fortney, J. J., Kempton, E. M.–R., et al. 2013, ApJ, 775, 33

Morley, C. V., Fortney, J. J., Marley, M. S., et al. 2015 ApJ, 815, 110

Pollack, J., Rages, K., Baines, K., et al. 1986, Icarus, 65, 442

Pruppacher, H. R. & Klett, J. D. 1978, Microphysics of Clouds and Precipitation (Dordrecht, D. Reidel Publishing Company)

Querry, M. R. 1987, Optical Constants of Minerals and Other Materials from the Millimeter to the Ultraviolet (Dover, NJ, U.S. Army Armament, Munitions Chemical Research)

Robinson, T. D., Stapelfeldt, K. R., & Marley, M. S. 2016, PASP, 128, 025003

Saumon, D., & Marley, M. S. 2008, ApJ, 689, 1327

Saumon, D., Marley, M. S., Abel, M., et al. 2012, ApJ, 750, 74

Schlawin, E., Zhao, M., Teske, J. K., et al. 2014, ApJ, 783, 5

Sing, D. K., Lecavelier des Etangs, A., Fortney, J. J., et al. 2013, MNRAS, 436, 2956

Sing, D. K., Fortney, J. J., Nikolov, N., et al. 2016, Nature, 529, 59

Spergel, D., Gehrels, N., Breckinridge, J., et al. 2013, arXiv:1305.5422

Toon, O. B., McKay, C. P., Ackerman, T. P., et al. 1989, J. Geophys. Res., 94, 16287

Torres, G. 2007, ApJ, 654, 1095

Trauger, J. T., Moody, D. C., Krist, J. E., et al. 2016, J. Ast. Inst. Sys., 2, 011013

van de Hulst, H. C. 1957, Light Scattering by Small Particles (New York, John Wiley & Sons, Inc.)

Wilkins, A. N., Deming, D., Madhusudhan, N., et al. 2014, ApJ, 783, 113

Zahnle, K., Marley, M. S., Morley, C. V., et al. 2016, ApJ, 824, 137

Software: FORTRAN, Python, IDL

ALL AUTHORS AND AFFILIATIONS

PETER GAO[1,2,3], MARK S. MARLEY, AND KEVIN ZAHNLE,
NASA Ames Research Center
Moffett Field, CA 94035, USA

TYLER D. ROBINSON[4,5],
Department of Astronomy and Astrophysics
University of California Santa Cruz
Santa Cruz, CA 95064, USA

AND

NIKOLE K. LEWIS.
Space Telescope Science Institute

Baltimore, MD 21218, USA

^{1}Division of Geological and Planetary Sciences, California Institute of Technology, Pasadena, CA 91125, USA,

^{2}NASA Postdoctoral Program Fellow,

^{3}pgao@caltech.edu,

^{4}Sagan Fellow,

^{5}NASA Astrobiology Institute's Virtual Planetary Laboratory